Assessment of the photocatalytic transformation of pyridinium-based ionic liquids in water

Assessment of the photocatalytic transformation of pyridinium-based ionic liquids in water.

Paola Calza*[1], Debora Fabbri[1], Giorgio Noè[1], Valentina Santoro[2], Claudio Medana[2]

[1] Departmemt of Chemistry, University of Torino, via P. Giuria 5, 10125, Torino, Italy.

[2] Department of Molecular Biotechnology and Health Sciences, University of Torino, via P. Giuria 5, 10125

*Corresponding author at: Department of Analytical Chemistry, University of Torino, via P. Giuria 5, 10125 Torino, Italy. Tel.: +39 011 6705268;fax: +39 011 6705242.

E-mail address: paola.calza@unito.it (P. Calza).

Abstract

We studied some ionic liquids (ILs) belonging to the pyridinium class under photocatalytic treatment. In particularly, we analysed how the length of the alkyl chain, the kind of inorganic ion and the type of substituents could influence the disappearance rate, the mineralization extent, the acute toxicity and the transformation mechanism. For such, we selected some pyridinium derivatives with different alkyl chain but the same anion, namely tetrafluoroborate (1-ethylpyridinium, 1-butylpyridinium, 1-hexylpyridimium), with two alkyl substituents (4-methyl-1-butylpyridium) and with a different substituent (1-cyanopropylpyridinium). Then, on a selected IL (1-butylpyridinium), we evaluate the role of different inorganic anions (bromine and chlorine). The results show that irrespective to the alkyl chain or the number of substituents, the transformation involved an attack to the alkyl chain, proceeded through the formation of harmless compounds and the mineralization was easily achieved within 4 h. Nitrogen was mainly released as ammonium ion. When introducing a cyano group, the extent of nitrate ions and the number of possible transformation route increased. Conversely, the type of inorganic ion deeply affected the transformation pathways and the extent of mineralization. Actually, in the presence of bromide as anion, IL was only partially mineralized and the formation of highly persistent transformation products occurred.

Keywords: TiO_2, pyridinium-based ionic liquids, photocatalysis, toxicity, transformation products

1. Introduction

Ionic liquids (ILs) at ordinary temperature are receiving considerable attention for application in different fields [1,2], i.e. lithium ion batteries [3], gas separation and handling [4,5], metal plating [6], dye sensitized solar cells, and as paint or polymer additives [7,8].

Due to their high stability, it can be expected in the near future the presence of significant amounts of ILs in wastewaters, with consequent further release into natural waters. If their low vapor pressure can preserve the atmosphere from the emission of toxic vapors, on the other hand their stability could make them hazardous to water and soil [9-12]. ILs partition in the environment is deeply influenced by their hydrophobicity. Surface water is the first environmental compartment in which ILs are spread as a result of industrial and laboratories waste. Therefore, we would expect to find more hydrophilic or polar ILs in surface water, while ILs with longer side chains could be distributed preferably in soils [13]. Hydrophobic ILs are linked to sediments and could behave as persistent pollutants, while hydrophilic ILs are more bioavailable [11]. Derivatives with short or hydroxylated chains are less adsorbed, but become more mobile in soils and can be issued more rapidly in surface waters and groundwater [14], causing contamination. The anionic component can influence adsorption as well as the cationic one; in particular ionic liquids endowed with anions able to form ion pairs show a greater adsorption in the soil [15].

Among the various biotic and abiotic transformation processes [16-18], photochemistry is a potentially important attenuation route influencing ILs fate in surface waters [19, 20]. Moreover, some studies showed that ILs are more toxic for cells in comparison to conventional solvents; in particular, the most common imidazolium based compounds showed high resistance toward microbial degradation [10].

Thus, it is important to develop efficient methods for a complete and safe ILs removal [21-23]. Recently, several studies describe the use of advanced oxidation processes towards ILs decomposition [24-31], while at present studies on the identification of their transformation product are scarce [30].

In this study, we investigated about the efficiency of heterogeneous photocatalysis toward the degradation of ILs holding different hydrophilicity and inorganic ions by assessing their transformation mechanisms and the extent of the mineralization process. The mutual influence of anion and cation was studied in detail. An hybrid linear trap-high resolution orbitrap was employed to identify the intermediate products formed during the course of ionic liquid degradation.

2. Experimental section

2.1. Materials and Reagents

1-Ethylpyridinium tetrafluoroborate (**EP-TFB**) (98%), 1-butylpyridinium bromide (**BP-Br**) (≥99%), 1-(3-cyanopropyl)pyridinium chloride (**CPP-Cl**) (98.5%), 1-butyl-4-methylpyridinium tetrafluoroborate (4-**BMP-**

TFB) (≥97,0%), acetonitrile(≥99.9%), formic acid(99%) and phosphoric acid were purchased from Sigma Aldrich, Milan, Italy.

1-Butylpyridinium chloride (**BP-Cl**) (99%), 1-butylpyridinium tetrafluoroborate (**BP-TFB**) (≥98%), 1-hexylpyridinium tetrafluoroborate (**HP-TFB**) (99%) and 1-butyl-3-methylpyridinium bromide (**3-BMP-Br**) (99%) were purchased from IoLiTec Ionic Liquids Technologies GmbH (Deutschland).

All aqueous solutions were prepared with ultrapure water Millipore Milli-Q^{TM}. TiO_2P25 (Evonik Industries, Italy) was used as photocatalyst.

2.2. Irradiation procedures

Irradiation experiments were performed in stirred cylindrical Pyrex cells containing 5 ml of aqueous dispersions with 20 mgL^{-1} of analyte and 200 mg L^{-1} of TiO_2. A Blacklight Philips TLK 05 (40W) lamp source with emission maximum at 360 nm was employed for irradiation. The dispersions at the end of the irradiation were filtered through 0.45 µM Millex LCR hydrophilic PTFE membranes (Millipore) before the analysis.

2.3. Analytical procedures

2.3.1. Liquid Chromatography-MS

All samples were analyzed by HPLC/HRMS. The chromatographic separations, monitored using an MS analyzer, were carried out with a Phenomenex Gemini NX C18 150 × 2.1 mm × 3 µm particle size (Phenomenex, Bologna, Italy), using an Ultimate 3000 HPLC instrument (Dionex, Thermo Scientific, Milan, Italy). The Injection volume was 20 µL and the flow rate 200 µL/min. The following gradient mobile phase composition was adopted: 5/95 to 95/5 in 27 min acetonitrile/5 mM heptafluorobutanoic acid in water.

A LTQ Orbitrap mass spectrometer (Thermo Scientific, Milan, Italy) equipped with an ESI ion source was used. The LC column effluent was delivered into the ion source using nitrogen as both sheath and auxiliary gas. The capillary voltage and tube lens voltage in the ESI source were maintained at 28 V and 70 V, respectively. The source voltage was set to 4.5 kV (in positive ion mode). The capillary temperature was maintained at 270°C. The acquisition method used was optimized beforehand in the tuning sections for the parent compound (capillary, magnetic lenses and collimating octapole voltages) to achieve maximum sensitivity. Mass accuracy of recorded ions (vs calculated) was ± 10 millimass units (mmu, without internal calibration).

Analyses were run using full scan MS (50-1000 *m/z* range), MS^2 acquisition in the positive ion mode, with a resolution of 30000 (500 *m/*z FWHM) in FTMS (full transmission) mode. The ions submitted to MS^2 acquisition were chosen on the base of full MS spectra abundance without using automatic dependent scan. Collision energy was set to 30 % for all of the MS^2 acquisition methods. MS^2 acquisition range was between the values of ion trap cut-off and *m/z* of the $(M+H)^+$ ion. Xcalibur (Thermo Scientific, Milan, Italy) software was used both for acquisition and data analysis.

2.3.2. Ion chromatography

A Dionex instrument equipped with a conductimeter detector was used. Cations were analysed with and a CS12A column using methanesulphonic acid (20 mM) as eluent at a flow rate of 1 mL min^{-1}. In such conditions, the retention time of the ammonium ion was 4.7 min. Anions were analysed with an AS9HC column and K_2CO_3 (9 mM) as eluent at a flow rate of 1 mL min^{-1}. Under these conditions, the retention times for nitrite and nitrate were 6.83 and 9.51, respectively.

2.3.3. Total organic carbon analyzer

Total organic carbon (TOC) was measured in filtered suspensions using a Shimadzu TOC-5000 analyzer (catalytic oxidation on Pt at 680°C). The calibration was performed using potassium phthalate standards.

2.3.4. Toxicity Measurements

The toxicity was evaluated with a Microtox Model 500 Toxicity Analyzer (Milan, Italy). Acute toxicity was evaluated with a bioluminescence inhibition assay using the marine bacterium *Vibrio fischeri* by monitoring changes in the natural emission of the luminescent bacteria when challenged with toxic compounds. Freeze-dried bacteria, reconstitution solution, diluent (2% NaCl) and an adjustment solution (non-toxic 22% sodium chloride) were obtained from Azur (Milan, Italy). Samples were tested in a medium containing 2% sodium chloride, in five dilutions, and luminescence was recorded after 5, 15, and 30 min of incubation at 15°C. Since no substantial change in luminescence was observed between 5 and 30 minutes, only the percent toxicity recorded at 15 minutes will be discussed. Inhibition of luminescence, compared with a toxic-free control to give the percentage inhibition, was calculated following the established protocol using the Microtox calculation program.

3. Results and discussion

3.1. Ionic liquids degradation and mineralization

Direct photolysis contribution was negligible for all ILs in the considered time window. Considering ILs degradation in the presence of TiO_2, Figure 1 shows ILs holding the same anion (BF_4^-), while Figure 2 displays ILs with different anions. Analyzing data of Fig. 1, **BP-TFB, HP-TFB** and **4-BMP-TFB** show easier disappearance than **EP-TFB** and their complete degradation occurred within 30 min. Compared to **EP-TFB**, the other three ILs examined show a wide time delay between the substrate disappearance (ca 30 min) and the complete mineralization (ca 120-150 min). The difference between the two curves has to be attributed to the TPs formation.

The release of nitrogen over time is very similar (and inverse) to TOC profile. Within 1 h, only a small percentage of nitrogen is released; afterward, a sharp increase was observed between one and 2 h and then the complete mineralization was achieved within 3h of irradiation. No nitrite traces were detected under the employed experimental conditions. The nitrogen reaches the stoichiometric amount within 2h and it is mainly released as ammonium ions in all cases (80-90%). Pyridine is known to degrade by giving aliphatic intermediates with one to five C atoms, all containing C=O groups. Whenever the N atom subsists, it is in amide form, so implying a prevalent conversion of nitrogen into ammonium [32]. Taking into account the nitrogen evolution, the formation of TPs more persistent than the parent compounds, still containing N in the structure, can be hypothesized.

The results obtained for **BP-Cl**, **BP-Br**, **BMP-Br** and **CPP-Cl** are reported in Figure 2. The two ILs with bromide present similar degradation curves and disappeared within 2h of treatment. Conversely, in the presence of bromide (**BP-Br** and **BMP-Br**), TOC profile was strongly modified and, even if a sharp decrease was achieved within 4 h of irradiation, at longer irradiation times (16 h) no more degradation occurred and almost 20% of the initial TOC persisted. The fate of nitrogen for **BP-Br** and **BMP-Br** was deeply modified as well. In the case of **BP-Br** the measured NH_4^+/NO_3^- ratio is close to 1, whereas the ammonium represents the most abundant product of nitrogen mineralization for **BMP-Br** degradation, for which the ratio is close to 3. For **BP-Br**, the stoichiometric release was not achieved, so implying that persistent TPs still containing the nitrogen were formed.

Analyzing **CPP-Cl**, the TOC disappearance was complete after 4h of irradiation and almost 85% was abated within 3h. The fate of nitrogen is rather interesting. Within 2h, nitrogen was mainly released as ammonium ions (55%), while for longer irradiation times it was released as nitrate ions. This behavior is well matched with the formation of cyanate at early stage, then slowly oxidized to give nitrate ion formation [33,34].

3.2. Acute toxicity

Acute toxicity was evaluated by monitoring changes in the natural emission of the luminescent bacteria *Vibrio fischeri*. Initially, EC_{50} values were calculated for all ILs and they are collected in Table 1. These values show a correlation between the number of carbons of the alkyl chain and the acute toxicity, as plotted in Figure 3. Analyzing ILs with the same anion (TFB), EC_{50} value increases from about 7 g/l for **EP-TFB**, holding two carbon atoms in the chain, to 95 mg/l for **HP-TFB**, with six carbon atoms, in agreement with literature data [35]. An increase of toxicity was also observed when a second aliphatic substituent (CH_3) is present in the aromatic structure, exhibiting an intermediate value between **BP-TFB** and **HP-TFB**.

166 The presence of a hydrophilic group (i.e. a cyano group) on butyl chain significantly decreases ILs toxicity, as
167 assessed by EC_{50} > 10 g/l. In fact, the lower hydrophobicity of the cation hinders the molecule capability to
168 pass through the cell membranes and exert acute toxicity on bacteria [35].

169 As reported in previous studies, the length of the alkyl chain had a significant influence on the toxicity of IL
170 and also the methyl groups appended to a pyridinium cation showed the same effect on toxicity [35].

171 Since the trend of increased growth inhibition with hydrophobicity had been demonstrated for other
172 microorganisms, the mechanism of toxicity of ILS may be explained through the membrane disruption
173 because of the ILs structural similarity to detergents, pesticides and antibiotics.

174 Another studies suggested mechanism of IL toxicity is related to acetylcholinesterase inhibition in more
175 complex test organisms [36 and references within].

176 Conversely, ILs toxicity was less influenced by the type of anion. For BP, the following order of toxicity was
177 observed: **BP-Br** <**BP-Cl** <**BP-TFB** in agreement with literature data [35].

178 Acute toxicity was monitored as well during the photocatalytic degradation for all of the compounds and the
179 percentage of inhibition effect is collected in Figure 4. For all ILs the initial inhibition percentage is worthless,
180 but a different toxicity is observed during the photocatalytic treatment.

181 The photocatalytic degradation of ILs holding TFB as inorganic ion proceeded through the formation of rather
182 harmless compounds. **EP-TFB** and **BMP-TFB** transformation proceeds through the formation of harmless
183 compounds as a very slight inhibition increase occured from 30 min onward (10-15%) TPs. While the presence
184 of short-chain groups seems to avoid the formation of harmful compounds, some toxicity was exhibited by
185 longer chain ILs **HP-TFB** and **BP-TFB** (inhibition percentages up to 30-40%),

186 As far as the behavior of **CPP-Cl,** initially it does not display any toxicity, but later on its transformation
187 proceeds through the formation of toxic compounds. The inhibition percentage increases up to 80 % after
188 60-120 min and then slows down. This trend closely resembles to the TPs temporal profiles as most of the
189 identified TPs greatly decrease from 120 to 240 min. So, it was not possible to assess which of the formed
190 TPs are the most hazardous.

191 For **BP-Br** and **BMP-Br** the toxicity increased from 15 min onward and became maximum after 4h of
192 irradiation. This could to be attributed to the formation of toxic and persistent TPs, whose formation has to
193 be ascribed to the presence of bromide as anion and is not directly related to the ILs organic moiety. As blank
194 analysis, a solution of NaBr was subjected to irradiation under the same experimental conditions aimed to
195 assess the contribution of bromide derivatives to the toxicity arising from photocatalytic treatment. As it can

196 be seen in the Figure S1, the toxicity increases with time of irradiation. Therefore, the detected toxicity has
197 to be chiefly ascribed to the formation of inorganic brominated species rather than to organic compounds.

198

199 **3.3. Characterization of transformation products**

200 TPs formed along with ILs photocatalysed degradation were detected *via* HPLC-MS, ESI positive mode.
201 Analyzing short chain ILs, 1-ethylpyridinium tetrafluoroborate (**EP-TFB**) shares with 1-cyanopropylpyridinium
202 chloride (**CPP-Cl**) several transformation routes as assessed in Scheme 1. **EP-TFB** transformation proceeds
203 through the formation of seven TPs, all already recognized during UV-B photolysis [20] and their MS and MS^2
204 ions are collected in Table S1. The recognized TPs involved hydroxylation (**TP-124** (1-
205 (hydroxyethyl)pyridinium) and **TP 140** (dihydroxylethyl-pyridinium)) hydroxylation/oxidation (**TP-122** and
206 **138**), detachment of the ethyl chain (**TP 80**, pyridinium ion) and ring opening (**TP 84**). The evolution profiles
207 over time for **EP-TFB** are shown in Figure 5. Most of TPs reached the maximum amount within 30-60 min,
208 with the only exception of **TP-138**. This is not surprising as its formation involved several steps, as assessed
209 by the transformation pathways collected in Scheme 1.

210 **CPP-Cl** transformation produced eleven TPs and their MS^2 ions are collected in Table S2, while the evolution
211 profiles over time are collected in Figure S2. Nine of them have been already detected under UV-B light and
212 their characterization is reported elsewhere [20]. They comprise **TP-163**, attributed to the monohydroxyl
213 derivative, **TP-136**, **TP-154** and **TP-152,** all formed through the detachment of the cyano group, **EP, TP-138**
214 and **TP-140** formed through the detachment of the methylcyano group. **TP-140** was formed through a bi-
215 hydroxylation, further transformed into **TP-138** through the oxidation of one of the two alcoholic groups to
216 a keto group; it matches with the monohydroxyl/keto derivative holding the OH group on the alkyl chain,
217 already detected with **EP-TFB**. **TP-94** and **TP-80** correspond to 1-methyl pyridinium ion and pyridinium ion,
218 respectively. Two additional TPs were detected during the photocatalytic treatment, **TP-130** and **TP-84**, both
219 involving the ring opening.

220 Butyl pyridinium derivatives share most of the formed TPs, but with some peculiar differences evidenced in
221 Scheme 2. **BP-TFB**, **BP-Cl** and **BP-Br** transformation involved the formation of fourteen, twelve and fifteen
222 TPs respectively. Three of them involved chain shortening (**TP-138** and **TP-140**) and chain detachment (**TP-**
223 **80**), and match with TPs already detected from **EP-TFB** and **CPP-Cl**. Their ions, detected by MS, are collected
224 in Table S3-S5, while the evolution profiles over time are collected in Figures S3-S5.

225 Considering **BP-Cl**, all the detected TPs match with those formed from **BP-TFB,** with only exception of **TP-**
226 **166-D**, and are completely degraded within 120 min. **TP-168-B**, **TP-134**, **TP-150C** and **TP-152B** were easily

formed and reached the maximum after 15 min of irradiation, while **TP-166-A** and **B** and **TP-80** achieved the maximum after 30 min; **TP-138** was slowly formed and is maximum at 60 min.

Following **BP-Br** degradation, the evolution profiles over time for most abundant and persistent TPs are reported in Figure 6, while the other TPs are collected in Figure S5. Almost all TPs disappears within 4h, with **TP-150-A** and **C** only exception, which persist and contribute to the lack of mineralization described in 3.1.

Three isobaric species at 152.1073 *m/z* with empirical formula $C_9H_{14}ON$ were formed and attributed to hydroxyl derivatives. In all cases, MS^2 spectra allowed to locate the OH group on the alkyl chain (**TP-152 A-C**).

Six isobaric species at 150.0892 *m/z* were detected and attributed to keto derivatives or hydroxylated with a double bound (**TP-150 A-F**). **TP-150-C** and **F** hold the keto group on the butyl chain, as assessed by the formation of the pyridinium ion in MS^2 spectrum. Furthermore, the loss of formaldehyde for **TP-150-F** allows to locate the keto group on C4. For the other isomers, no specific information can be deduced by MS^2 spectra.

Three isobaric species at 168.1025 *m/z* were formed and attributed to bi-hydroxyl derivatives (**TP-168-A-C**). For **TP-168-A** and **B**, both OH groups are located on the alkyl chain. In the case of **TP-168-B** the loss of methanol combined with the loss of $C_2H_6O_2$ suggested to locate the two OH groups on the C3 and C4. For **TP-168-C** an OH group was located on C3 (loss of C_2H_4O combined with the absence of methanol loss).

Four species at 166.0867 *m/z* were detected and attributed to the bihydroxylated/oxidized compounds; in all cases, the groups were located on the alkyl chain. **TP-166-A** exhibits the loss of formaldehyde, so permitting to assess the presence of the carbonyl group on C4. Reasonably, it comes from the oxidation of the species **TP-168-C**.

A TP with 134.0967 *m/z* (**TP-134**) could be attributed to the formation of a double bond in the chain or to the chain closure to give a ring. MS^2 is not useful to assess which of the two routes occurred.

Scheme 3 collects TPs formed from **4-BMP-TFB** and **3-BMP-Br**, while their evolution profiles as a function of irradiation time are shown in Figure S6 and 7, respectively. Thirty-two TPs were detected during **4-BMP-TFB** degradation, all summarized in Table S6, eighteen of which already recognized and characterized during the UV-B photolysis [20]. **3-BMP-Br** transformation proceeds through the formation of nineteen TPs, all collected in Table S7.

Both compounds share some transformation pathways involving oxidation and/or oxidation and the side chain reduction, but they show also some peculiar routes. First of all, the presence of bromide as anion leads again to the formation of some highly persistent TPs. Secondly, the position of methyl group on the pyridine ring seems to affect the extent of different pathways. With **4-BMP-TFB** TPs formed at higher amount comes

from hydroxylation (**TP-182**), reduction (**TP-148**) and reduction/hydroxylation (**TP-164**). For **3-BMP-Br**, **TPs-164-B,D,F** were the most prominent. **TP-164** and **TP-150** were particularly persistent and these should be the same structures already evidenced from **BP-Br** plus a methyl group. Besides, while for **4-BMP-TFB** the detachment/shortening of alkyl chains prevails, for **3-BMP-Br** this route is absent and only the ring-opening occurred.

Analyzing different TPs, a first group of TPs comprises mono and dihydroxylated derivatives and their oxidation products. Four or two monohydroxyl derivatives with 166**.**1233 *m/z* (**TP-166-A-D** for **4-BMP-TFB** and **TP-166-E,F** for **3-BMP-Br**) were formed. **TP-166-E,F** were recognized also during biodegradation [37]. For isomer **D** the OH group can be located on the butyl chain [20], while for **TP-166-C** on C_2 or C_3 due to the loss of C_3H_6O. In both cases the absence of methanol loss in MS^2 spectra allowed to exclude a hydroxylation on C4.

Twelve isobaric species with *m/z* 164.1078 and empirical formula $C_{10}H_{14}ON$ (**TP-164**) were formed from **4-BMP-TFB** and **3-BMP-Br**. Nine of them matched with keto derivatives, four of which already detected *via* direct photolysis (**TP-164-A**, **C**, **D** and **F**) [20]. For **TP**-**164-B** the loss of C_3H_6 permitted to exclude the presence of a keto group on C2-C4. For **164-E** the loss of C_2H_4O allowed to locate the keto group on C3. **TP-164-B, G and I** were well matched with the presence of a double bond in the alkyl chain plus an hydroxyl group.

Two species rather stable were formed with 162.0891 and 148.1126 *m/z*. For **TP-162** (formed from **4-BMP-TFB**), the most abundant ion exhibited in MS^2 the loss of C_4H_4; this peculiar loss allowed to propose an insaturation/cyclization of the butyl chain. Conversely, **TP-162** produced from **3-BMP-Br** presented 3-methylpyridinium as product ion in MS^2 spectrum, thus allowing to locate an oxygen on the butyl chain. **TP-148-A-C** with empirical formula $C_{10}H_{14}N$ presented an insaturation/cyclization as well; **TP-148-A** and **C,** losing acetylene, suggested the presence of a double bond on C3-C4 on the butyl chain.

Six dihydroxyderivatives with 182.1184 *m/z* were formed from **4-BMP-TFB**; isomers **B**, **C** and **D** were also formed during direct photolysis [20]. For **3-BMP-Br**, only three isomers (**TP-182-G,H, I**) were detected. **TP-182-A** holds an OH group on butyl chain and the other one on the ring, as assessed by the product ion C_6H_8ON. For **TP-182-F** the losses of C_2H_6O and $C_3H_7O_2$ allowed to position the two OH groups on C2 and C3. This hypothesis is confirmed by the loss of CO in MS^3 spectra. For TP-**182-E** no structurally-diagnostic ions were present in MS^2 spectrum. **TP-182-G** holds the two OH groups on carbon 3 and 4 thanks to the loss of methanol and $C_2H_3O_2$. This was further confirmed by the formation of 3-methylpyridiun as product ion (*m/z* 94.0655). For **TP-182-H**, the loss of C_4H_8 permitted to exclude a hydroxylation on the butyl chain.

Eight bihydroxylated/oxidized **4-BMP-TBF** with 180.0995 *m/z* were formed, three of them already detected *via* direct photolysis (**TP-180-A**,**C** and **E**) [20]. **TP-180-F** holds both groups on the butyl chain. **TP-180-B** and **H** hold a keto group on the butyl chain and the OH group on the other part of the molecule, as assessed by the

loss of C_4H_6O in MS^2 spectrum. **TP-180-D** could hold the keto group on the methyl or butyl C4, as due the formaldehyde loss; the combined loss of H_2O in MS^2 and formaldehyde in MS^3 permitted to exclude the involvement of the methyl group. **3-BMP-Br** produced an isomer only (**TP-180-I**), also detected via biodegradation [37]. It was further oxidized to produce **TP-178** with *m/z* 178.0869 and empirical formula $C_{10}H_{12}O_2N$.

Three compounds at *m/z* 134.0967, 150.0891 and 168.0996 were formed through the detachment of the methyl group and were only detected from **4-BMP-TFB**. **TP-134** presented a double bond (or a ring closure). **TP-150** showed a demethylation and a carbonyl group; its intensity was too low to permit MS^2 analysis. **TP-168** involved a demethylation and a bihydroxylation.

For **4-BMP-TFB** only, two TPs involving chain shortening and two hydroxyl group were detected (**TP-154)**. MS^2 product ions did not allow to properly locate them. **TP-124** could be formed by the detachment of the butyl chain together with the methyl oxidation and hydroxylation. For **3-BMP-Br**, **TP-94** matched with 3-methylpyridinium, confirmed by the injection of a standard solution and already detected via biodegradation [37].

Few TPs involved the ring opening and the first one was **TP-102** with *m/z* 102.0912 and empirical formula $C_5H_{12}ON$ that involved ring opening and hydroxylation. The formation of a compound at 76.0391 *m/z* with empirical formula $C_2H_6O_2N$ occured and its formation involved the pyridinium ring opening. **TP 84** with *m/z* 84.0806 and empirical formula $C_5H_{10}N$, derived from ring opening and partial of alkyl chain conservation.

1-Hexylpyridinium tetrafluoroborate (**HP-TFB**) produced 46 TPs, whose MS and MS^2 ions are collected in Table S8 and 9 and the proposed structure are shown in Scheme 4. TPs temporal profiles are plotted in Figure S8.

The main TPs were **TP-196-D** and **TP-180**, implying mono and dihydroxylation, and **TP-162**, involving a reduction on the alkyl chain. Besides, the pathways involving the chain shortening, chain detachment and ring cleavage played a minor role. **HP-TFB** shares with other ILs **TP-80** (pyridinium ion), formed though the detachment of alkyl chain, three species characterized by chain shortening, mono or dihydroxylation and oxidation (**TP-148**, **TP-166** and **TP 140**) and two TPs involved the ring opening, namely **TP-84** and **TP-102**. Furthermore, two TPs **TP-154** and **TP-152** with empirical formula $C_8H_{12}O_2N$ and $C_8H_{10}O_2N$ were in common with TPs coming from **CPP-Cl** transformation and involved chain shortening, hydroxylation and oxidation.

Analyzing **HP-TFB** peculiar TPs, the first group comprises mono, di and trihydroxylated/oxidized derivatives. Nine isobaric species with *m/z* 178.1234 and empirical formula $C_{11}H_{16}ON$ (**TP-178**) were formed. Isomers **178-B, C, D, E** and **G** hold the keto group on the alkyl chain. Furthermore, in the case of **TP-178-B**, the loss of C_2H_4O, combined with the absence of formaldehyde loss, allowed us to locate the group on C5. In all cases,

the formation of the pyridinium ion (*m/z* 80.0492) as product ion allowed us to locate the OH group on the alkyl chain. The fragmentation of TP-178-F and G can be justified by the hydroxylation of parent molecule and oxidation of alkyl chain, whereas no useful information to elucidate the structure of TP-178A and B was obtained.

Five isobaric species with *m/z* 196.1341 (**TP-196**) and empirical formula $C_{11}H_{18}O_2N$, were detected and attributed to bihydroxylated-HP. **TP196-A** and **196-C**, hold both OH groups on the alkyl chain, as assessed by the product ion at 80.0460 *m/z*; furthermore, the loss of C_2H_6O, combined with the absence of the methanol loss, permits to locate one of the two hydroxyls on the C5. Ten isobaric species with 194.1187 *m/z* and empirical formula $C_{11}H_{16}O_2N$ (**TP-194**) were formed and attributed to bihydroxylation/oxidation processes. Two isobaric species with *m/z* 192.1030 and empirical formula $C_{11}H_{14}O_2N$ (**TP-192**), due to a bihydroxylation/oxidation process were then detected. Two **TP-210** and a **TP-208** were detected and involved trihydroxylation with oxidation of one (or two) hydroxyl group to keto groups; the formation of pyridinium ion in their MS^2 allows to locate these groups in the alkyl chain.

The second group comprises **TP-162, TP-160** and **TP-176** with empirical formula $C_{11}H_{16}N$, $C_{11}H_{14}N$ and $C_{11}H_{14}ON$, respectively, that are well matched with structure holding double bond(s) in the alkyl chain.

It can be concluded that the type of anion does not influence deeply the degradation pathway of ILs and all BP share most of the intermediates arising from mono and dihydroxylation of molecule and detachment of the alkyl chain. The presence of TPs showing the alkyl chain shortening is peculiar for **BP-TFP**, **BP-Cl**, **EP-TFB** and **CPP-Cl**, whereas in the case of **BP-Br** the formation of TPs holding the keto group on the butyl chain was observed. Also for ILs with a second alkyl chain (i.e a methyl group), the main pathways of degradation are hydroxylation, reduction and reduction/hydroxylation. On the other hand, the presence of a longer chain involves the formation of TPs of holding double bond(s) in the alkyl chain.

Conclusions

In the case of ILs containing TFB as anion, even if some differences in the time trend occurred, neither the alkyl chain length or the presence of more than one substituent does significantly affect the mineralization process. In all cases, the complete mineralization was easily achieved within 2-3 h of irradiation and nitrogen is mainly released as ammonium ions. Conversely, for ILs with bromide as anion, a lack of mineralization was assessed.

All ILs share some transformation pathways but present also some peculiar routes. In the case of **4-BMP-TFB** and **3-BMP-Br**, TPs formed at higher amount comes from hydroxylation (**TP-182**), reduction (**TP-148**) and reduction/hydroxylation (**TP-164-B**). Compared to other ILs, the mechanism of reduction plays a key role in

355 the **HP-TFB** degradation, with the formation of TPs holding two double bonds in the alkyl chain, while the
356 ring opening plays a minor role. The three BP ILs share most of the transformation pathways, with some
357 differences. **BP-TFB** and **BP-Cl** exhibit a chain shortening with the formation of **TP-138** and **TP-140**, two
358 transformation products already recognized from **EP-TFB** and **CPP-Cl**. Conversely, **BP-Br** degradation formed
359 some persistent TPs.

360 The photocatalytic degradation of ILs holding TFB as inorganic ion proceeded through the formation of rather
361 harmless compounds, while **CPP-Cl**, **BP-Br** and **3-BMP-Br** transformation involved the formation of hazardous
362 products.

363

364 **Acknowledgments**

365 We acknowledge support by MIUR, in the frame of the collaborative international consortium
366 WATERJPI2013-MOTREM of the "Water Challenges for a Changing World" Joint Programming Initiative
367 (WaterJPI) Pilot Call.

368

369 **References**

370 [1] N. V. Plechkova and K. R. Seddon, Applications of ionic liquids in the chemical industry, Chem. Soc. Rev.
371 37 (2008) 123-150.
372 [2] J. D. Holbrey and K. R. Seddon, Ionic liquids, Clean Technol. Environ. 1 (1999) 223-236.
373 [3] M. Galiński, A. Lewandowski, I. Stępniak, Ionic liquids as electrolytes, Electrochim. Acta 51 (2006) 5567-
374 5580.
375 [4] D. J. Tempel, P. B. Henderson, J. R. Brzozowski, R. M. Pearlstein, H. Cheng, High gas storage capacities for
376 ionic liquids through chemical complexation, J. Am. Chem. Soc. 130 (2008) 400-401.
377 [5] T. Predel and E. Schlücker, Ionic Liquids in Oxygen Compression, Chem. Eng. Technol. 32 (2009) 1183-
378 1188.
379 [6] Q. X. Liu, S. Z. E. Abedin, F. Endres, Electroplating of mild steel by aluminium in a first generation ionic
380 liquid: A green alternative to commercial Al-plating in organic solvents, Surf. Coat. Technol. 201 (2006) 1352-
381 1356.
382 [7] R. Kawano, H. Matsui, C. Matsuyama, A. Sato, M. A. B. H. Susan, N. Tanabe, M. Watanabe, High
383 performance dye-sensitized solar cells using ionic liquids as their electrolytes, J. Photochem. Photobiol. A,
384 164 (2004) 87-92.
385 [8] B. Weyershausen, K. Lehmann, Industrial application of ionic liquids as performance additives, Green
386 Chem. 7 (2005) 15-19.
387 [9] S.D. Richardson, T.A. Ternes, Water analysis: emerging contaminants and current issues, Anal. Chem. 86
388 (2014) 2813-2848.
389 [10] T.P.T Pham, C.-W. Cho, Y.-S. Yun, Environmental fate and toxicity of ionic liquids: a review, Water
390 Research 44 (2010) 352-372.
391 [11] M.C. Bubalo, K. Radošević, I.R. Redovniković, J. Halambek, V.G. Srček, A brief overview of the potential
392 environmental hazards of ionic liquids, Ecotox. Environ. Safe. 99 (2014) 1-12.
393 [12] M. Czerwicka, S. Stolte, A. Müller, E. M. Siedlecka, M. Golebiowski, J. Kumirska, P. Stepnowski,
394 Identification of ionic liquid breakdown products in an advanced oxidation system., J. Hazard. Mater. 171
395 (2009) 478-483.
396 [13] J. J Beaulieu, J. L. Tank, M. Kopacz, Sorption of imidazolium-based ionic liquids to aquatic sediments,
397 Chemosphere 70 (2008) 1320-1328.
398 [14] M. Amde, J.F. Liu, L. Pang, Environmental application, fate, effects and concerns of ionic liquids: a review,
399 Environ. Sci. Technol. 49 (2015) 12611-12627.
400 [15] M. Matzke, K. Thiele, A. Müller, J. Filser, Sorption and desorption of imidazolium based ionic liquids in
401 different soil types, Chemosphere 74 (2009) 568-574.

402 [16] L. Ford, J. R. Harjani, F. Atefi, M. T. Garcia, T. D. Singer, P.J. Scammells, Further studies on the
403 biodegradation of ionic liquids, Green Chem. 12 (2010) 1783-1789.
404 [17] D. Coleman and N. Gathergood, Biodegradation studies of ionic liquids, Chem. Soc. Rev. 39 (2010) 600-
405 637.
406 [18] A. Jordan and N. Gathergood, Biodegradation of ionic liquid-a critical review, Chem. Soc. Rev 44 (2015)
407 8200-8237.
408 [19] P. Calza, D. Vione, D. Fabbri, R. Aigotti, C. Medana, Imidazolium-based ionic liquids in water: Assessment
409 of photocatalytic and photochemical transformation, Environ. Sci. Technol. 49 (2015) 10951-10958.
410 [20] P. Calza, G. Noè, D. Fabbri, V. Santoro, C. Minero, D. Vione, C. Medana, Photoinduced transformation of
411 pyridinium-based ionic liquids, and implications for their photochemical behavior in surface waters,
412 submitted to Water Research.
413 [21] S. Stolte, S. Steudte, A. Igartua, P. Stepnowski, The biodegradation of ionic liquids–the view from a
414 chemical structure perspective, Curr. Org. Chem. 15 (2011) 1946–1973.
415 [22] N. Banić, M. Vraneš, B. Abramović, J. Csanádi, S. Gadžurić, Thermochromism, stability and
416 thermodynamics of cobalt(II) complexes in newly synthesized nitrate based ionic liquid and its photostability,
417 Dalton Trans. 43 (2014) 15515 -15525.
418 [23] K. R. Seddon, Ionic Liquids for Clean Technology, J. Chem. Technol. Biotechnol. 68 (1997) 351-356.
419 [24] M. Munos, C.M. Dominguez, Z.M. de Pedro, A. Quintanilla, J.A. Casas, J.J. Rodriguez, Ionic liquids break
420 down by Fenton oxidation, Catalysis Today 240 (2015) 16-21.
421 [25] E.M. Siedlecka, W. Mrozik, Z. Kaczynski, P. Stepnowski, Degradation of 1-butyl-3-methylimidazolium
422 chloride ionic liquid in a Fenton-like system, J. Hazard. Mater. 154 (2008) 893-900.
423 [26] P. Stepnowski, A. Zaleska, Comparison of different advanced oxidation processes for the degradation of
424 room temperature ionic liquids, J. Photochem. Photobiol., A 170 (2005) 45-50.
425 [27] T. Itakura, K. Hirata, M. Aoki, R. Sasai, H. Yoshida, H. Itoh, Decomposition and removal of ionic liquid in
426 aqueous solution by hydrothermal and photocatalytic treatment, Environ. Chem. Lett. 7, (2009) 343-345.
427 [28] E. M. Siedlecka, P. Stepnowski, The effect of alkyl chain length on the degradation of alkylimidazolium-
428 and pyridinium-type ionic liquids in a Fenton-like system, Environ. Sci Pollut. Res. 16 (2009) 453–458.
429 [29] E. M. Siedlecka, A. Wieckowska, P. Stepnowski, Influence of inorganic ions on MTBE degradation by
430 Fenton's reagent, J. Hazard. Mater. 147 (2007) 497-502.
431 [30] A. Pieczynska, A. Ofiarska, A. F. Borzyszkowska, A. BiałkBielinska, P. Stepnowski, S. Stolte, E. M. Siedlecka,
432 A comparative study of electrochemical degradation of imidazolium and pyridinium ionic liquids: A reaction
433 pathway and ecotoxicity evaluation, Sep. Purif. Technol. 156 (2015) 522-534.
434 [31] E. M. Siedlecka, S. Stolte, M. Gołębiowski, A. Nienstedt, P. Stepnowski, J. Thöming, Advanced oxidation
435 process for the removal of ionic liquids from water: The influence of functionalized side chains on the
436 electrochemical degradability of imidazolium cations, Sep. Purif. Technol. 101 (2012) 26-33.

[32] P. Calza, E. Pelizzetti, C. Minero, The fate of the organic nitrogen in photocatalysis. An overview, J. Appl. Electrochem. 35 (2005) 665-673.

[33] V. Augugliaro, J. Blanco Galvez, J. Caceres Vasquez, E. Garcia Lopez, V. Loddo, M.J. López-Muñoz, S. Malato Rodriguez, G. Marcì, L. Palmisano, M. Schiavello, J. Soria Ruiz, Photocatalytic Oxidation of Cyanide in Aqueous TiO_2 Suspensions Irradiated by Sunlight in Mild and Strong Oxidant Conditions, Catal. Today 54 (1999) 245-253.

[34] S.N. Frank and A.J. Bard, Heterogeneous photocatalytic oxidation of cyanide ion in aqueous solutions at titanium dioxide powder, J. Am. Chem. Soc. 99 (1977) 303-304.

[35] S. Viboud, N. Papaiconomou, A. Cortesi, G. Chatel, M. Draye, D. Fontvieille, Correlating the structure and composition of ionic liquids with their toxicity on *Vibrio fischeri*: A systematic study, J. Hazard. Mater. 215–216 (2012) 40– 48.

[36] K. M. Docherty, Jr. C. F. Kulpa, Toxicity and antimicrobial activity of imidazolium and pyridinium ionic liquids, Green Chem. 7 (2005) 185–189.

[37] T. P. T. Pham, C.W. Cho, C.-O. Jeon, Y.-J. Chung, Y.-S. Yun, Identification of metabolites involved in the biodegradation of the ionic liquid 1-Butyl-3-methylpyridinium Bromide by Activated Sludge Microorganisms, Environ. Sci. Technol. 43 (2009) 516-521.

Figure captions

Figure 1. ILs disappearance curves, TOC evolution profile and inorganic ions release over time for ILs with BF_4^- as anion (**EP-TFB** 1-ethylpirydinium, **BP-TFB** 1-butylpiridinium, **HP-TFB** 1-hexylpyridinium, **4-BMP-TFB** 1-butyl-4-methylpyridinium).

Figure 2. ILs disappearance curve, TOC evolution profile and inorganic ions release over time for ILs with other anions (**BP-Cl** 1-butylpyridinium chloride, **BP-Br** 1-butyl-pyridinium bromide, **3-BMP-Br** 1-butyl-3-methylpyrimidium bromide and **CPP-Cl** 1-cyanopropyl chloride).

Figure 3. Relation between $Log_{10}(EC_{50})$ (mg/l) and the number of carbon on alkyl chains**.**

Figure 4. Acute toxicity for ILs during the photocatalytic treatment; (top) **EP-TFB**, **BP-TFB**, **HP-TFB**, **BMP-TFB**; (bottom) **BP-Cl**, **BP-Br**, **BMP-Br** and **CPP-Cl**.

Figure 5. Transformation products formed from compound **EP-TFB** degradation in the presence of TiO_2.

Figure 6. Persistent and more abundant transformation products formed from compound **BP-Br** degradation in the presence of TiO_2.

Scheme 1. Proposed transformation pathways followed by compound **EP-TFB** and **CPP-Cl** in the presence of TiO_2 (200 mg/l).

Scheme 2. TPs formed from butyl-pyridine (**BP-TFB**, **BP-Cl**, **BP-Br**). TPs formed from all BP derivatives are marked with one asterisk, with two those formed from **BP-Cl** and **BP-TFB** only, with three those with **BP-Br** only, with four in the case of **BP-Br** and **BP-TFB** only, with five the TPs for **BP-TFB** only and with six asterisks the one obtained from **BP-Br** and **BP-Cl** only.

Scheme 3. Proposed transformation pathways followed by **4-BMP-TFB** and **3-BMP-Br** under photocatalytic treatment. With one asterisk are indicated TPs formed from **4-BMP-TFB** only and with two the ones TPs formed from **3-BMP- Br** only.

501 **Scheme 4.** Proposed transformation pathways followed by **HP-TFB** under photocatalytic treatment.

502 **Table 1.** EC_{50} values for the investigated ILs.

503

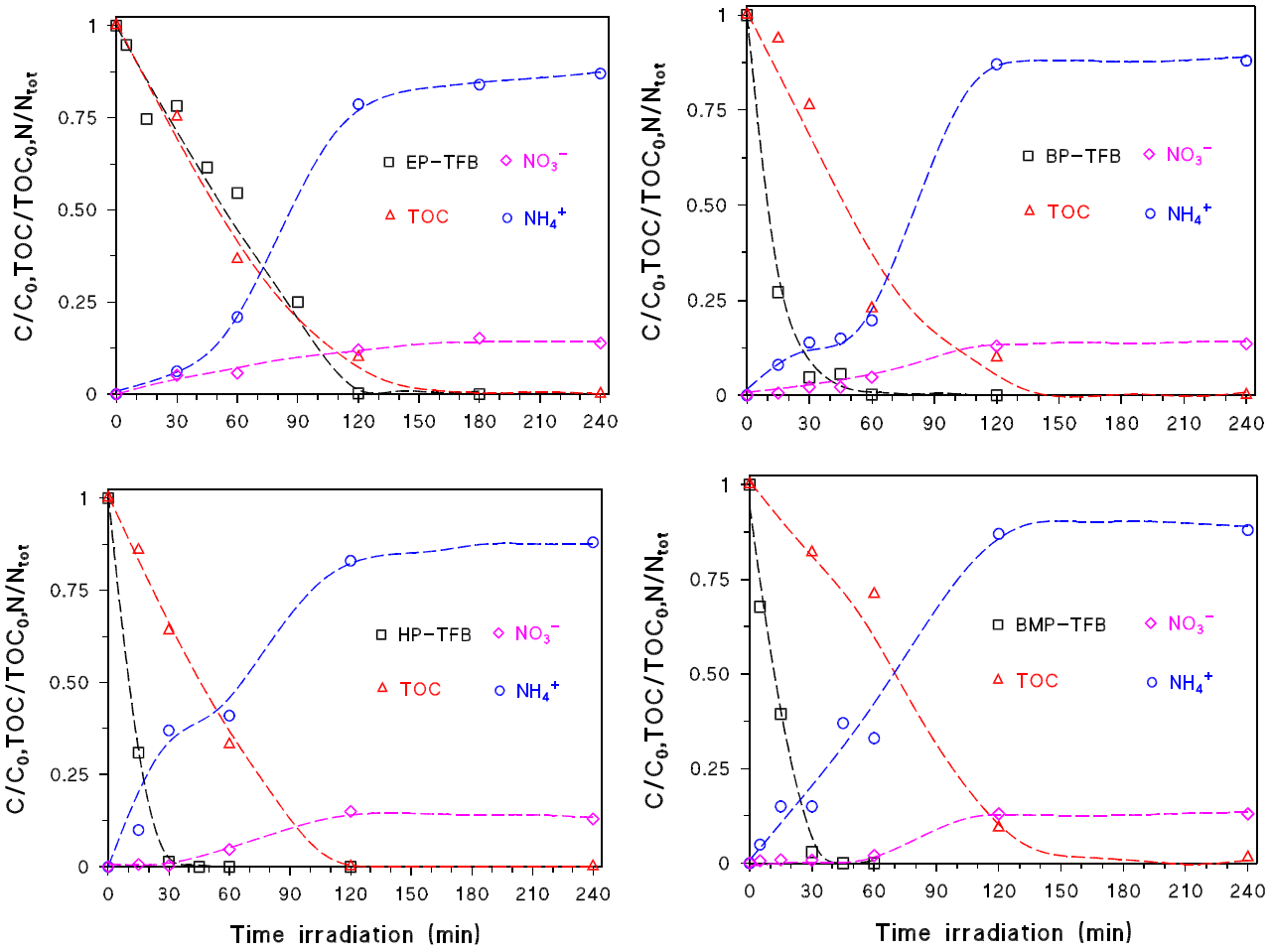

504

505 **Figure 1**.

506

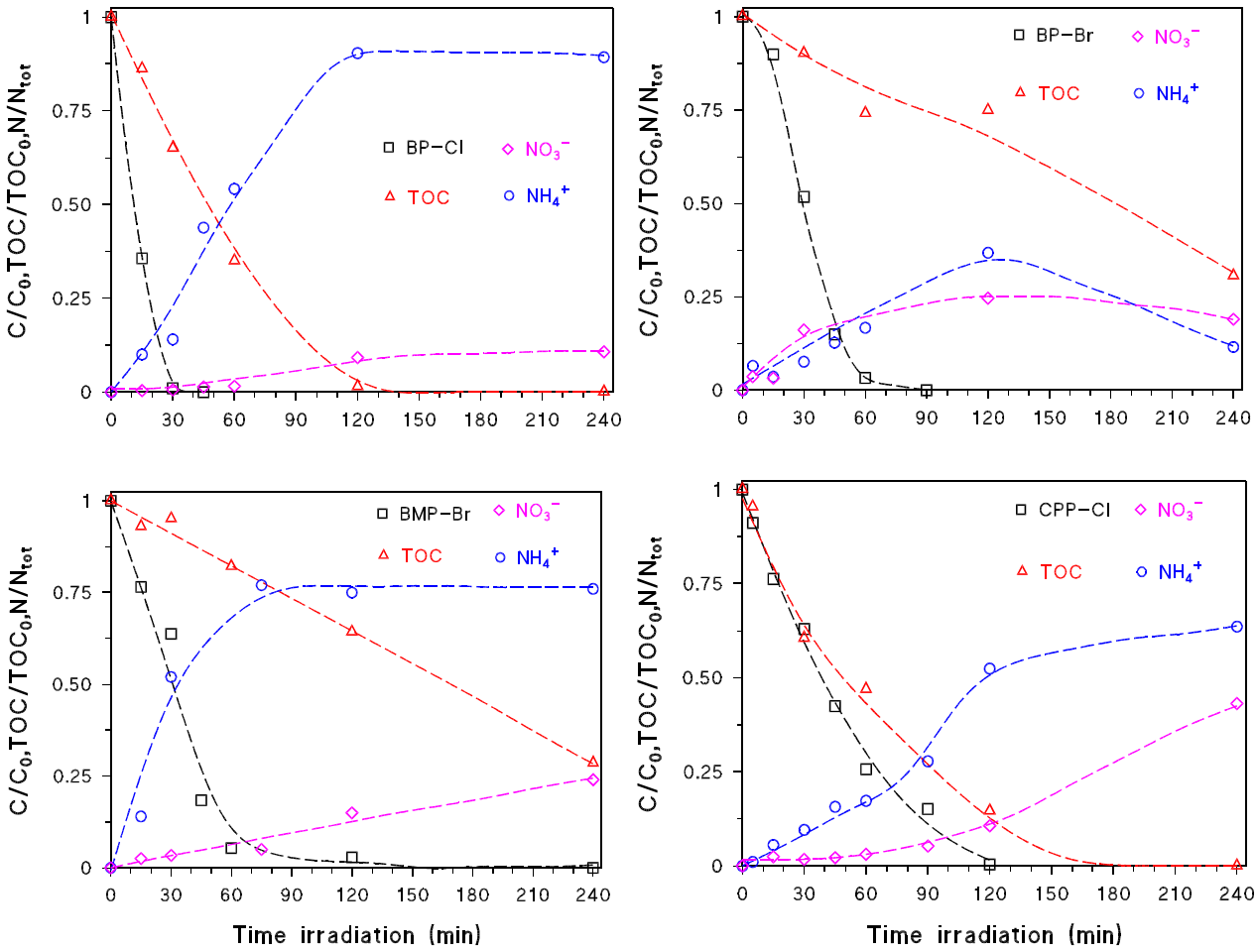
C/C0,TOC/TOC0,N/Ntot
BP−Cl
BP−Br
BMP−Br
CPP−Cl
NO3−
NH4+
TOC
Time irradiation (min)

Figure 2.

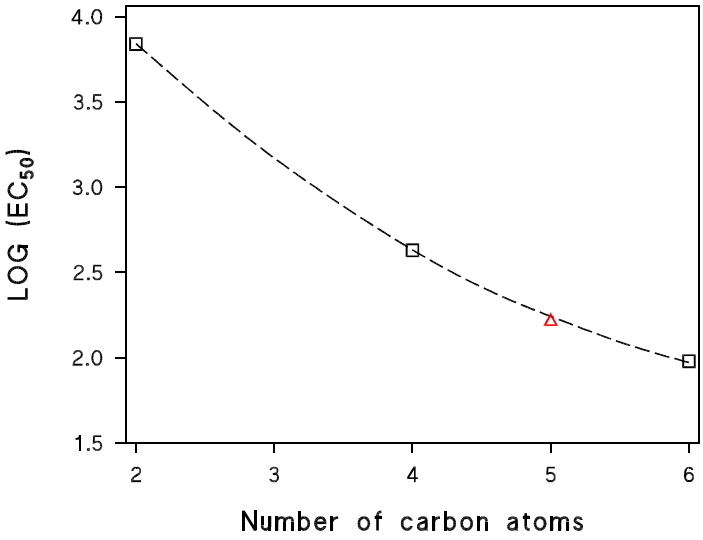

511

512 **Figure 3.**

513

514

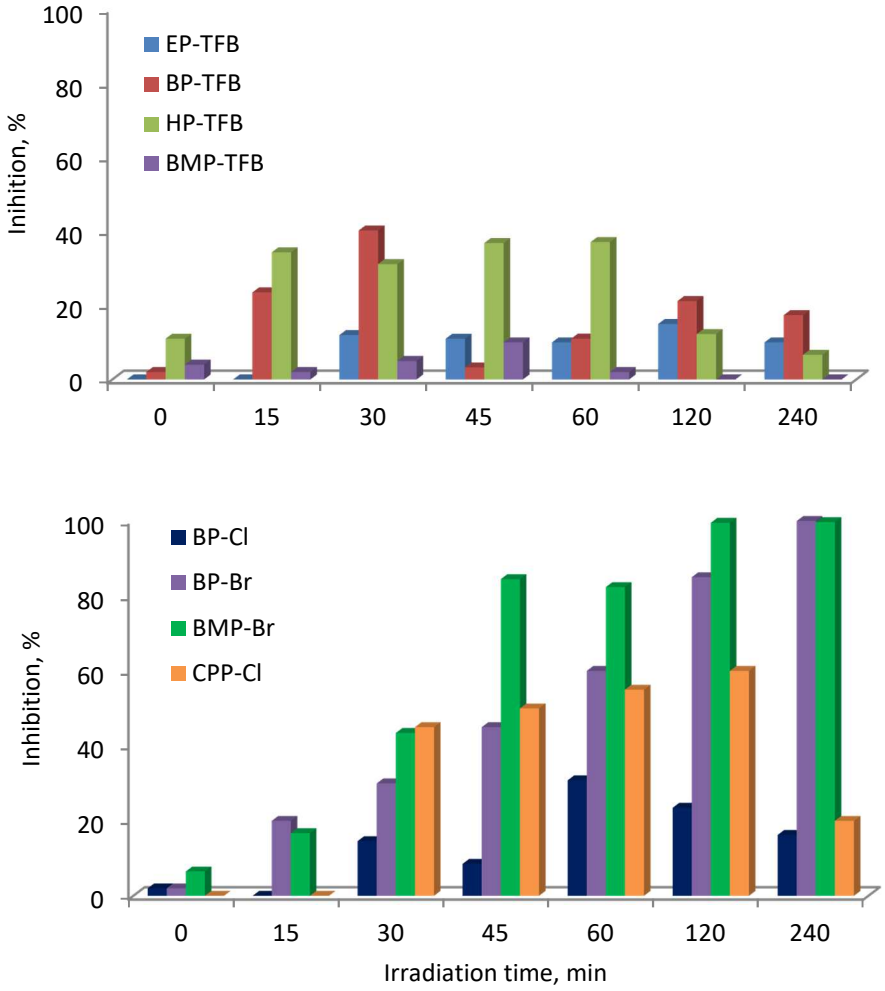

515

516 **Figure 4**.

517

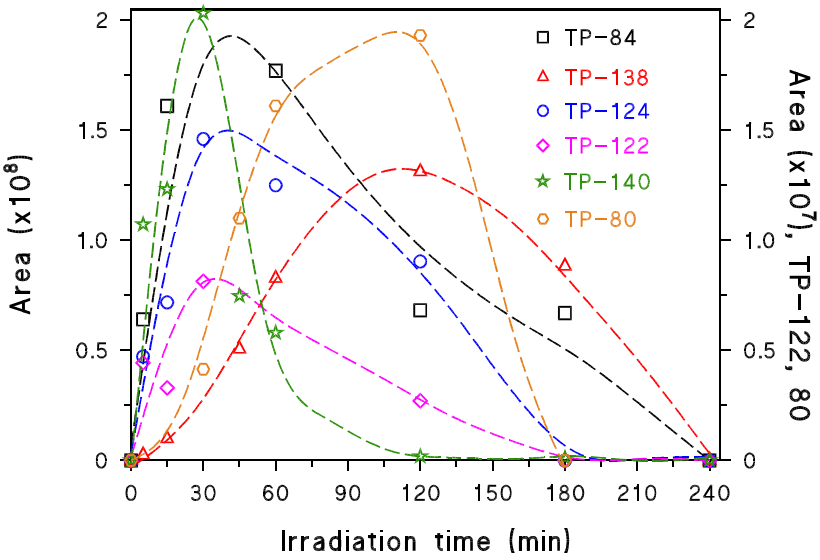

518

519 **Figure 5**.

520

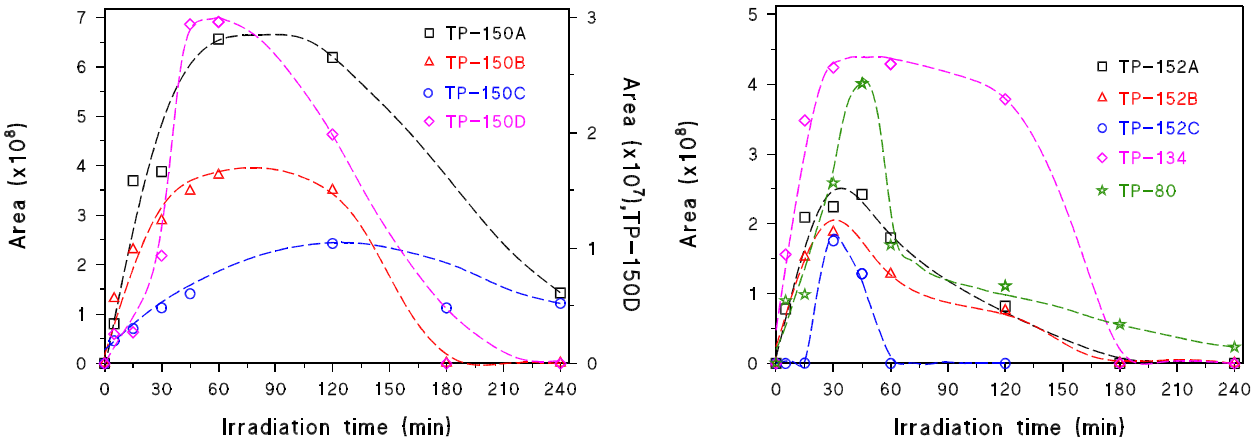

521

522 **Figure 6**.

523

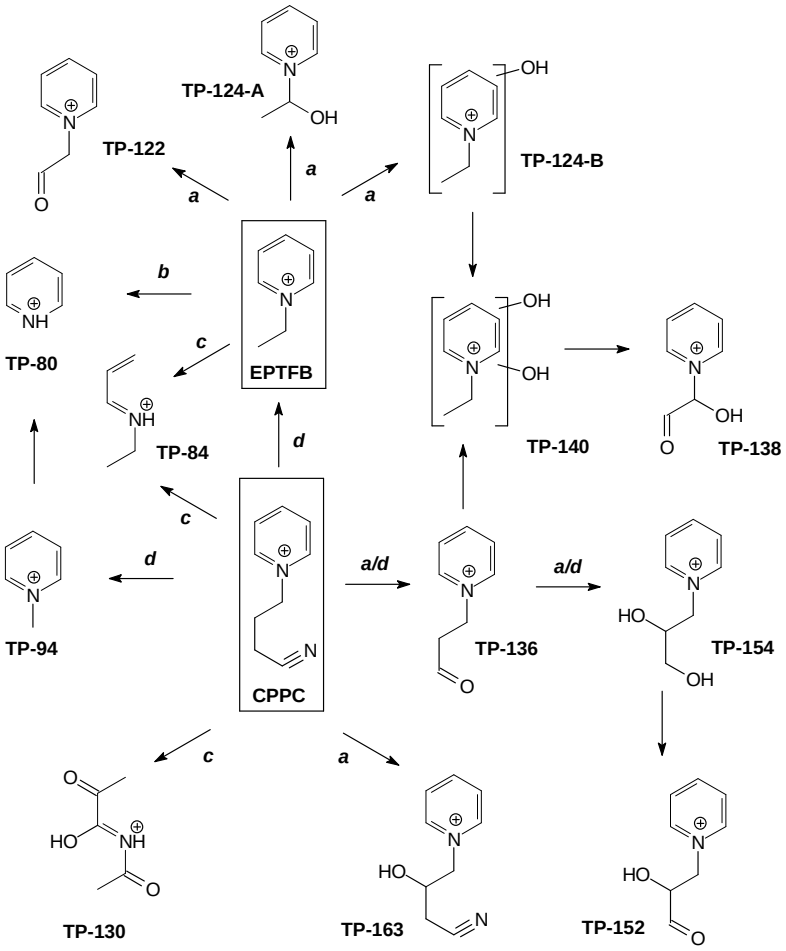

524

525 **Scheme 1.**

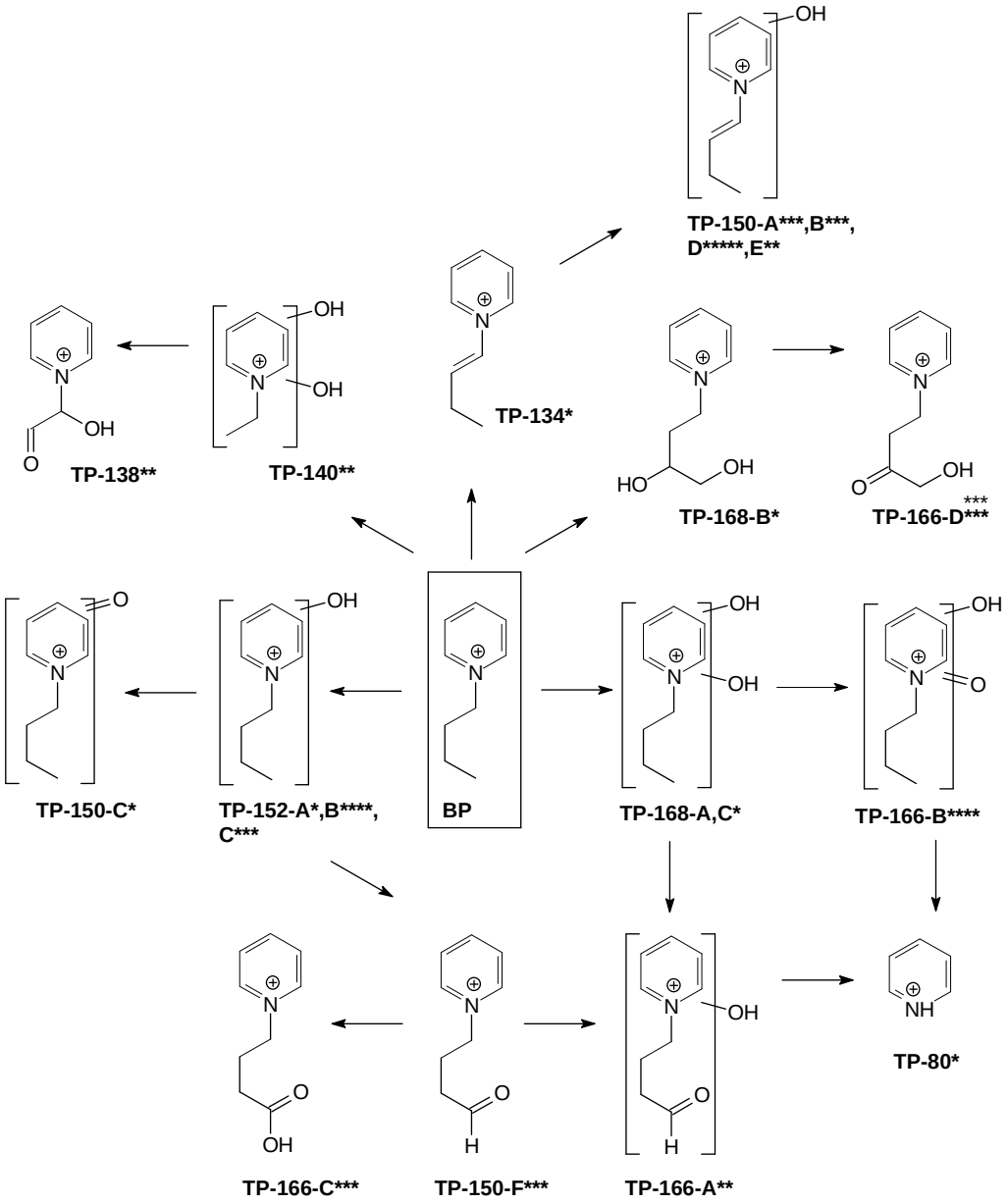

526

527 **Scheme 2**.

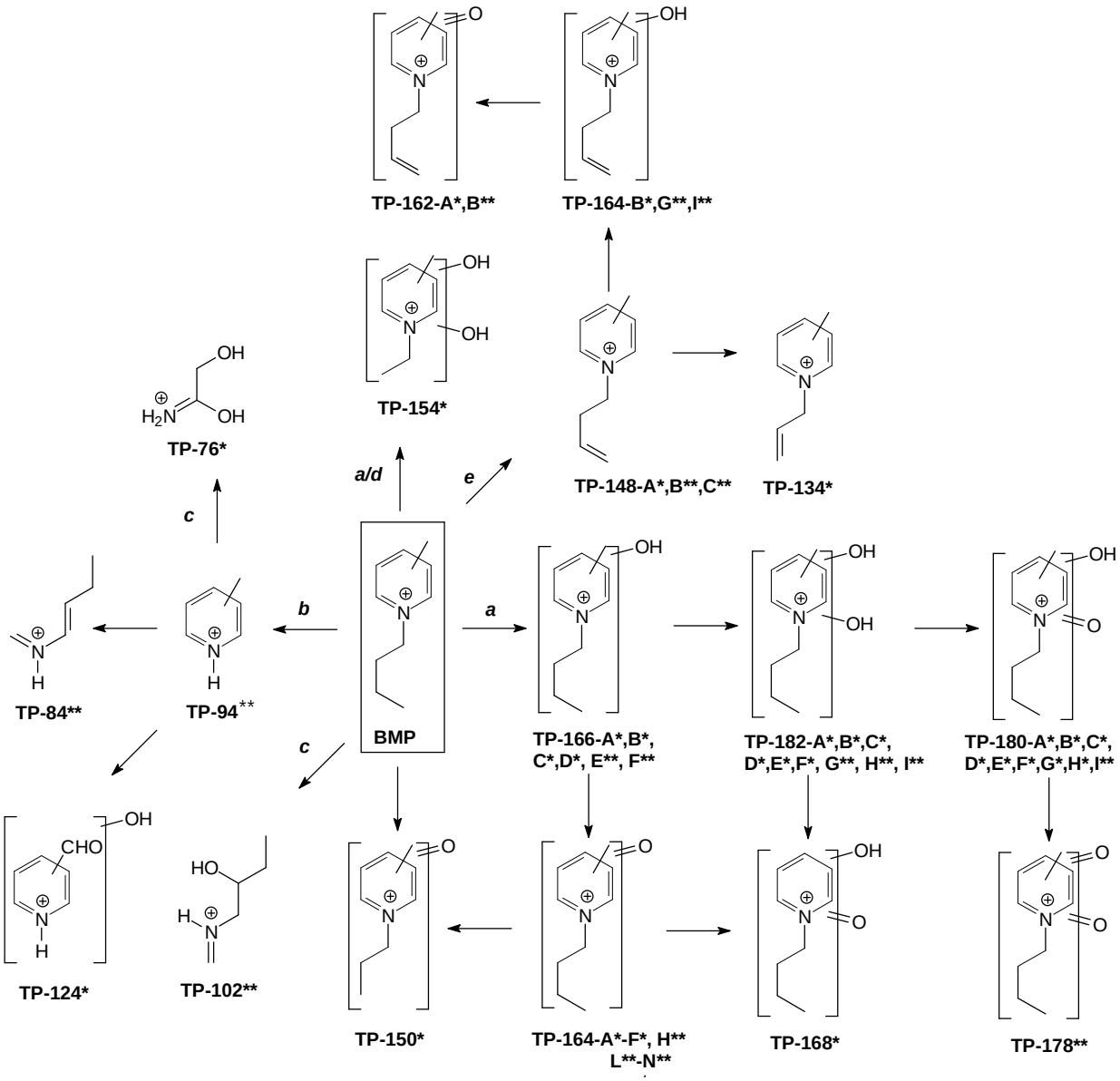

528

529 **Scheme 3.**

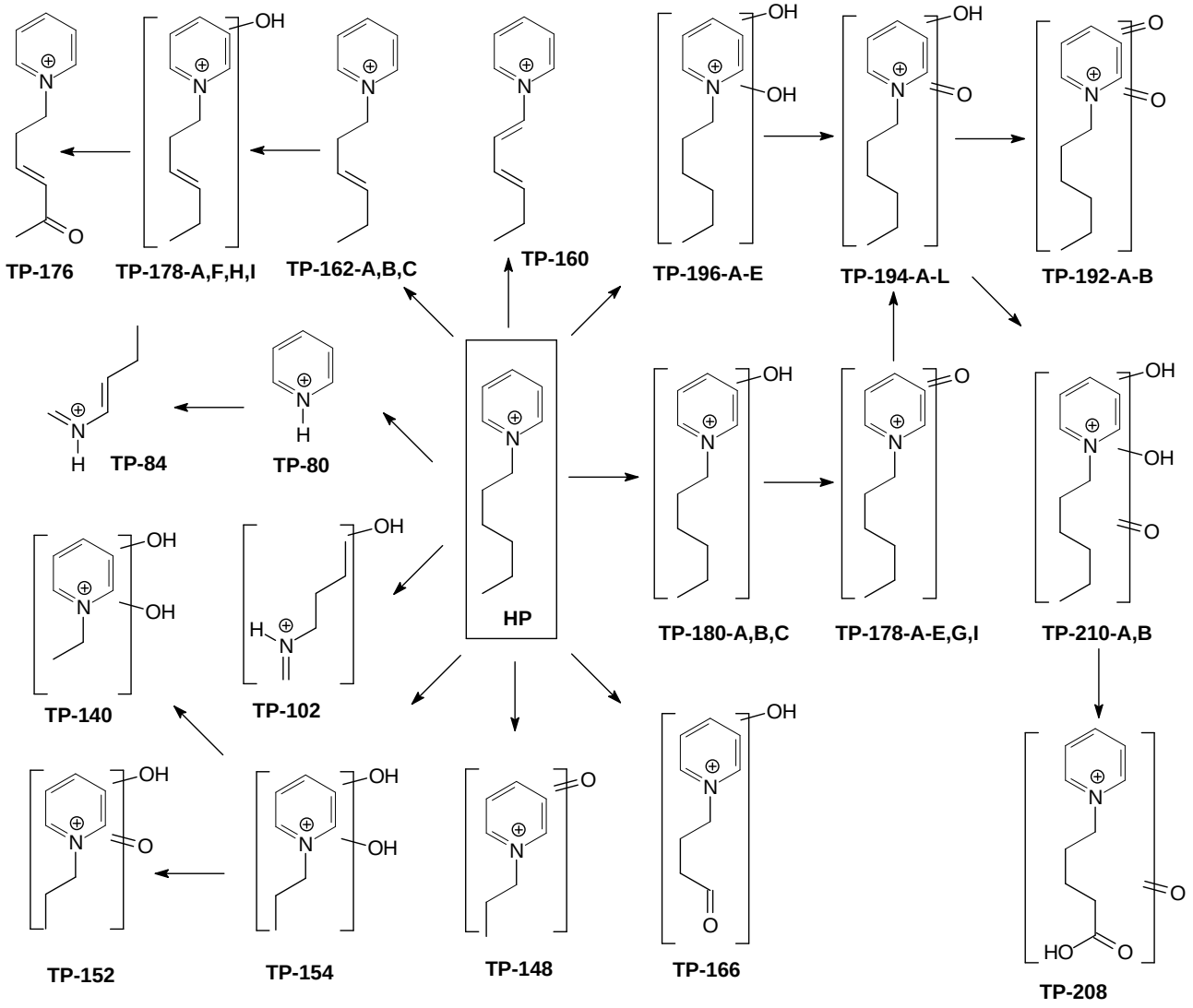

530

531 **Scheme 4.**

532

533 **Table 1.** EC50 values for the investigated ILs.

	EP-TFB	**BP-TFB**	**BP-Cl**	**BP-Br**	**BMP-TFB**	**BMP-Br**	**HP-TFB**	**CPP-Cl**
EC50 (mg/L)	6988	423,5	494,6	539,6	164,0	139,04	94,89	>10000

534